NANO LETTERS

2007
Vol. 7, No. 12
3645−3649

Localized Current Injection and Submicron Organic Light-Emitting Device on a Pyramidal Atomic Force Microscopy Tip

Yiying Zhao,[†] Kwang H. An,[‡] Shuo Chen,[†] Brendan O'Connor,[‡] Kevin P. Pipe,[‡] and Max Shtein*,[†]

Department of Materials Science and Engineering, Department of Mechanical Engineering, The University of Michigan, Ann Arbor, Michigan 48109-2125

Received August 1, 2007

ABSTRACT

An organic light-emitting device was fabricated on a commercial atomic force microscopy (AFM) probe having a pyramidal tip by a lithography-free vacuum thermal evaporation (VTE) process. The line-of-sight molecular transport characteristic of VTE results in controlled thickness variation across the nonplanar substrate, such that localized current injection occurs at the tip region. Furthermore, the high curvature of the AFM tip vertex concentrates the electric field, causing highly localized bipolar charge injection, accompanied by photon emission from a region less than a micrometer across. This light source exhibits a range of features potentially attractive for applications such as probe-based optical microscopy, nanoscale light sensing, and chemical detection.

Nanoscale light sources have enjoyed intense interest in the past decade due to their potential applications in quantum communications, near-field scanning optical microscopy (NSOM),[1] nanoscale photolithography, and detection. Among those applications, NSOM is the most well-developed one, and it has been applied in the study of microelectronic,[2−3] photonic,[4−5] surface plasmon-polariton,[6] biological,[7] and molecular systems.[8] A traditional NSOM probe tip is an optically pumped device that couples a far-field source to a sample through a hollow pyramid or through a pulled optical fiber with a partially etched metal cladding. Some of the limitations in this optically pumped technique include low optical transmission efficiency,[9] heating of the tip,[10−11] and poor reproducibility of probe fabrication.[12] The combination of these and other factors impedes achieving a higher resolution or integration with other on-chip applications.

Figure 1 conceptually illustrates a different approach in which an electrically pumped nanoscale light source is realized on the tip of a conventional atomic force microscopy (AFM) probe, potentially overcoming some of the limitations of conventional probe microscopy. This article has two aims. First, it describes in detail the enabling probe structure, its operating principles, and a fabrication approach. Second, it it shows a method for spatially controlling electrical carrier injection or removal from an organic optoelectron device, using built-in fields caused by nanoscale surface features on nonplanar substrates.

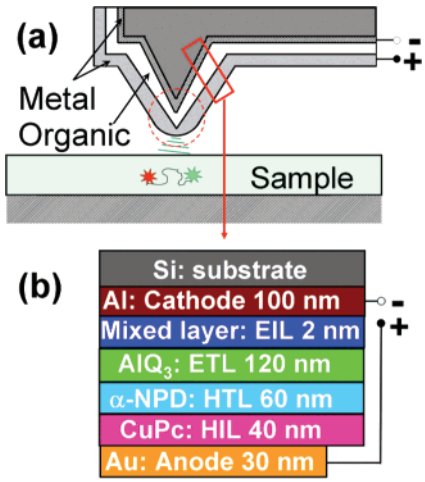

Figure 1. (a) An illustration of the concept of an electrically pumped nanoscale light source, fabricated using a conventional AFM probe as a substrate. **(b)** The device structure used in this experiment: Al (100 nm)/LiF/Al/Alq_3 mixed layer (2 nm)/Alq_3 (120 nm)/α-NPD (60 nm)/CuPc (40 nm)/Au (30 nm). All the layer thickness are measured based on those layers on the base of AFM probe.

Several efforts toward integrating an electrically pumped light source with an AFM probe have been reported,

* Corresponding author. E-mail: mshtein@umich.edu.
[†] Department of Material Science and Engineering.
[‡] Department of Mechanical Engineering.

10.1021/nl071883w CCC: $37.00
Published on Web 11/03/2007

concentrating mainly on group III−V semiconductors.[13,14] Sasaki et al.[13] have demonstrated a multifunctional probe that integrates a light-emitting diode (LED), waveguide, and aperture. Because this device couples the LED light to the aperture via a waveguide, the source is still in the far field. This results in waveguiding losses and low signal-to-noise ratio. Heisig et al.[14] have integrated a gallium arsenide (GaAs) cantilever with an electrically pumped GaAs LED. However, use of GaAs as the cantilever material complicates device fabrication, while light emission in the infrared limits the scope of application. Generally, high-efficiency, crystalline light-emitting materials are typically direct-gap III−V or II−VI compound semiconductors and have poor lattice-matching to common scanning probe substrates, the vast majority of which are fabricated using silicon-based micro electrochemical system (MEMS) technology.[15−16] It is this inherent difficulty in integrating the two inorganic material systems that prompted an investigation into combining organic light-emitting devices (OLEDs) with micromachined silicon cantilevers.

Previously, we reported on the fabrication of a circular OLED on a flat silicon cantilever, using a combination of vacuum thermal evaporation (VTE), vapor-phase deposition, and ion beam lithography.[17] The ring-shaped light emission region formed on the cantilever was several micrometers in diameter and approximately one micrometer in thickness. However, both the planar geometry of the working part of the probe and the distance ($\sim$1 μm) from the recessed light-emitting region to the probe surface limit the ability to position the light source within nanometers of a sample. Furthermore, the fabrication sequence included a chemical vapor deposition step and a time-consuming ion beam-milling procedure, requiring additional tooling and sample transfers. Here, we demonstrate a new device geometry (Figure 1a) that is much simpler to fabricate and whose operating mechanism allows a considerably smaller emissive region.

Consider an OLED structure consisting of molecular organic thin films sandwiched between two metallic electrodes, as depicted in Figure 2a. Under forward bias, electrons and holes are injected from the metallic electrodes and recombine inside the organic film, emitting photons through a semitransparent electrode. At low bias, charge conduction occurs in the space charge-limited regime. The onset of light emission in this structure occurs at higher bias in the trapped charge-limited regime, the transition to which typically has a strong threshold behavior with voltage.[18] The threshold voltage, in turn, increases with the thickness of the organic layers,[18] an effect that can be utilized here to control the location of light emission in the proposed device.

Consider now the OLED structure deposited onto a typical AFM probe tip by VTE and the effect of the pyramidal probe tip geometry, as illustrated in Figure 2b. The organic material is evaporated from a resistively heated cell onto a substrate mounted in the center of a rotating stage, positioned at a vertical distance H and horizontal distance R from the evaporation source. Because of the rectilinear molecular trajectories during VTE,[19] the deposited layer thickness varies

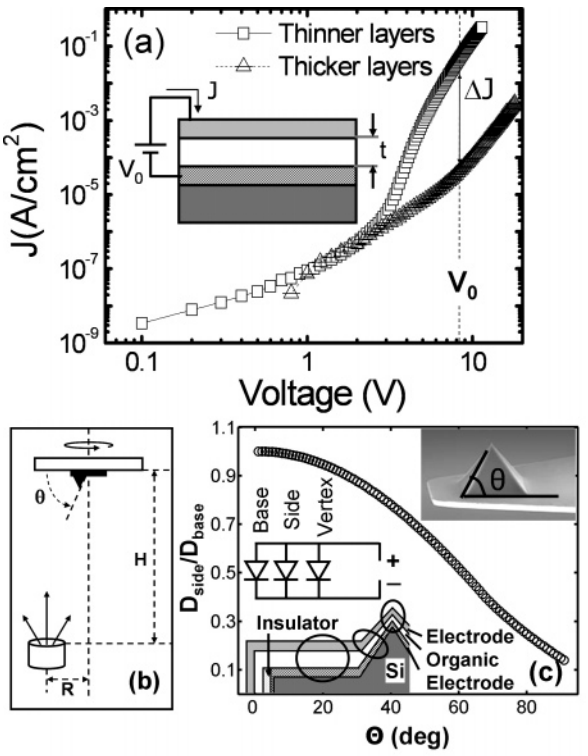

Figure 2. **(**a**)** A plot of the current density (J) vs applied voltage (V) for an archetypal OLED structure, showing the higher current density at constant bias in the trapped charge-limited transport regime for the thinner organic layers. **(b)** A diagram illustrating the geometry of a typical laboratory VTE deposition system. **(**c**)** (Top right inset) SEM image of an AFM pyramidal probe, where θ is defined as the angle between the sides of a pyramidal tip (side) and the flat portion of the probe "base". (Main image) A plot of the relative layer thickness (D_{side}/D_{base}) as a function of the angle θ in our VTE system. (Bottom left inset) An illustration of the cross-section of the organic heterojunction device fabricated on AFM probes in VTE and the equivalent circuit model developed on the device architecture and layer thickness.

with the angle of incidence of molecules on the surface, resulting in thinner layers on the sloping sides of the pyramidal tip of the AFM probe compared to those on the base (Figure 2c). Under constant bias, the current density in the pyramidal region will be considerably higher than that on the flat portion of the probe ("base").

To predict the ratio of the layer thickness on the inclined sides of the pyramidal tip (D_{side}) relative to the base region (D_{base}) we plot the ratio D_{side}/D_{base} in Figure 2c as a function of the angle θ between the sides of the pyramidal tip and the plane of the substrate holder. (We also account for the horizontal offset of the source cell and the AFM probe during the deposition.)[19] For $\theta = 60°$ for example, to obtain a 100 nm thick organic layer on the sides of the pyramid, a nominally 200 nm thick film is deposited. Note that the plot also predicts that the side-walls of the AFM probe are coated with a film that is much thinner than elsewhere on the probe. To avoid the shunting of electrical current through the thin organic film on the side-walls, an insulating compound can be separately deposited to coat the cathode with the back of the probe facing the evaporation source. The entire resulting heterostructure device deposited on the probe can be thought

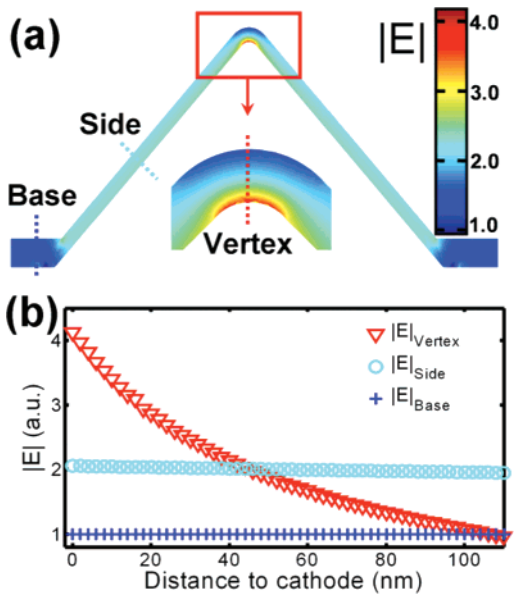

Figure 3. **(a)** The cross-section of the electric field contour across the whole device on the AFM probe. The electric field strength is normalized to that inside of the material on the base of the pyramid. The electric field vanishes inside of both metal electrodes. **(b)** A plot of the electric field intensity across the thickness of the layers at the vertex, the side, and the base.

of as a combination of several devices sharing a common anode and cathode, namely, three diodes electrically connected in parallel (see the inset of Figure 2c). The three diodes correspond to the organic heterostructure on the base, the side, and the vertex, while the insulator-coated sidewall region of the probe can be treated as a large resistor. By carefully choosing the layer thickness, the difference between the threshold voltages of two diodes can be made as large as 5−7 V, and the corresponding difference in current density can be 3−5 orders of magnitude, allowing for localized current injection at the pyramid, in turn resulting in localized light emission.

Importantly, further localization of current and light emission is possible due to the presence of nanoscale curvature of the substrate, namely, the sharp vertex of the pyramid. A typical tip curvature for silicon- and silicon nitride-based AFM tips is 50 nm (data from Veeco Inc.), resulting in a concentrated built-in electric field at the vertex relative to a planar surface. The resulting electric field distribution inside the device deposited on the AFM probe can be calculated by solving Maxwell's equations using finite element analysis. Because of the similar dielectric constants of all the organic layers used here, the organic stack can be treated as a single dielectric layer; the electric field is assumed to vanish inside both metal electrodes. Charge accumulation at the metal−organic and organic−organic interfaces can be neglected for the purpose of this analysis.

The results of this analysis are shown in Figure 3a, which maps the electric field distribution across the probe as a color map. The probe is shown in cross-sectional view; the field intensity is normalized to the intensity inside the organic layers on the base of the pyramid. Figure 3b compares the magnitude of the electric field strength inside the device at the vertex, the sides of the pyramid, and the base of the AFM probe. The concentration of the field at the vertex is clearly evident and amounts to 2.1 times that on the sides of the pyramid and 4.3 times that on the base. This effect is strong (hence its extensive use in nanoscale electron emission devices)[20] and must be considered in designing the layer sequence of the electrically pumped heterostructure device. The concentrated electric field can be used here to further localize charge injection in an organic-based optoelectronic device.

The direction of the electric field favors electron ejection from the tip region and thus requires the conventional OLED layer sequence to be reversed. The cathode and electron transport layers must be deposited first, followed by hole injection and anode layers. This is in contrast to the majority of planar OLED devices, in which holes are injected from the substrate side and electrons are injected from the top-deposited cathode. Nevertheless, the reversed layer sequence is feasible[21−22] (also shown earlier in Figure 1b) and in conjunction with the high curvature of the tip is expected to help localize light emission.

To experimentally demonstrate the device concept described above, a silicon nitride pyramidal AFM probe (NP-UC, Vecco Probes) was chosen as the substrate (see inset of Figure 2c). The square base of the pyramidal tip measured 5 μm, while the interior angle between the side of the pyramid and the substrate, θ, was approximately 60 degrees. The OLED layers were vacuum-deposited onto the probe and consisted of 100 nm thick aluminum cathode, 2 nm thick mixed layer of Al, LiF, and Alq_3, 120 nm thick layer of Alq_3, 60 nm thick layer of α-NPD, 40 nm thick layer of CuPc, and 30 nm thick layer of gold. An electrically insulating layer consisting of 300 nm thick layer of LiF was vacuum-deposited from the back of the probe following the cathode. (All layer thicknesses correspond to the base portion of the probe and are approximately a factor of 2 thinner on the inclined sides of the pyramidal tip, as indicated earlier in Figure 2c. The current−voltage ($I-V$) characteristic of the device was measured using an Agilent 4156B semiconductor parameter analyzer, while the electroluminescence (EL) and optical images of the device were captured using an optical microscope having a long working distance (20.5 mm) objective (50×, numerical aperture of 0.42), and a charge-coupled device (CCD) camera.

Figure 4 shows a plot of current divided by cathode area vs voltage ($I/A-V$) of two devices having identical layer structures deposited onto commercial AFM probe structures. In one device, the layers were deposited onto a probe substrate with the cantilever intact (device A); in another device, the layers were deposited onto a probe substrate with the cantilever removed (device B) (see insets of Figure 4). The plot of I/A vs V, which accounts for the incidental difference in cathode coverage area between the two devices, indicates that the current density in the structure with the cantilever intact (device A) is higher due to the presence of the tip. In fact, the average current in the structure with the tipped cantilever is 2 to 3 orders of magnitude greater than that in the control, suggesting that the majority

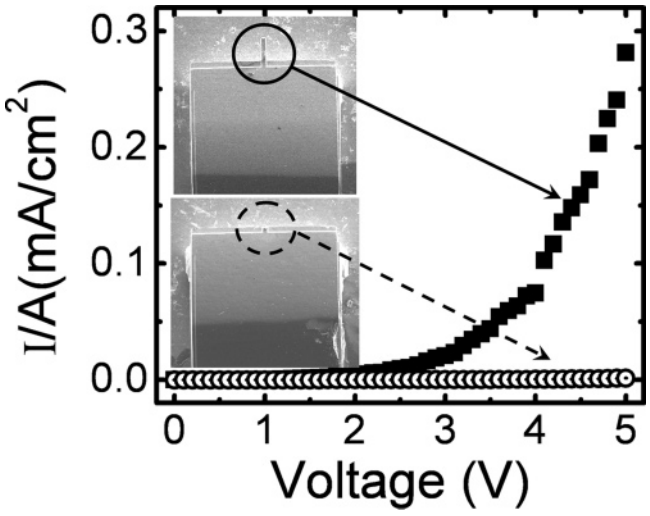

Figure 4. A plot of the average current vs driving voltage ($I/A-V$) for two organic heterojunction devices having identical structures, deposited on AFM probes, one with the pyramidal tip intact and one without (as shown in SEM images as the inset). The current density is estimated by dividing the total probe current by the cathode area (light gray in the inset image).

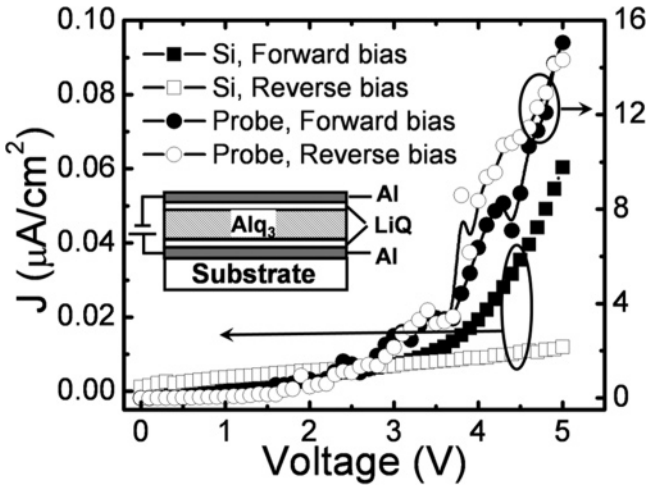

Figure 5. A plot of the average current density vs voltage of a unipolar injection device on a planar silicon substrate and an AFM probe. (Inset) Device structure used to evaluate the effect of electric field on electron injection, the structure is substrate/bottom electrode Al (100 nm)/LiQ (8-hydroxy-quinolinato lithium 2 nm)/Alq_3 (120 nm)/LiQ (2 nm)/top electrode Al (100 nm).

of the current in the cantilever extension is carried by the pyramidal region and not by the flat portion or by possible leakage paths.

We now experimentally examine the effect of electric field concentration on charge injection in the pyramidal region of the probe. First, we account for the effect of deposition sequence on charge injection. To do so, we use a layer structure that permits unipolar charge injection, deposited onto a planar substrate and on the pyramidal tip. The layer structure is shown in the inset of Figure 5, along with the corresponding current density vs voltage ($J-V$) characteristics in forward and reverse bias. The layer sequence consisted of planar Si substrate, bottom electrode Al (100 nm), LiQ (8-hydroxy-quinolinato lithium 2 nm), Alq_3 (120

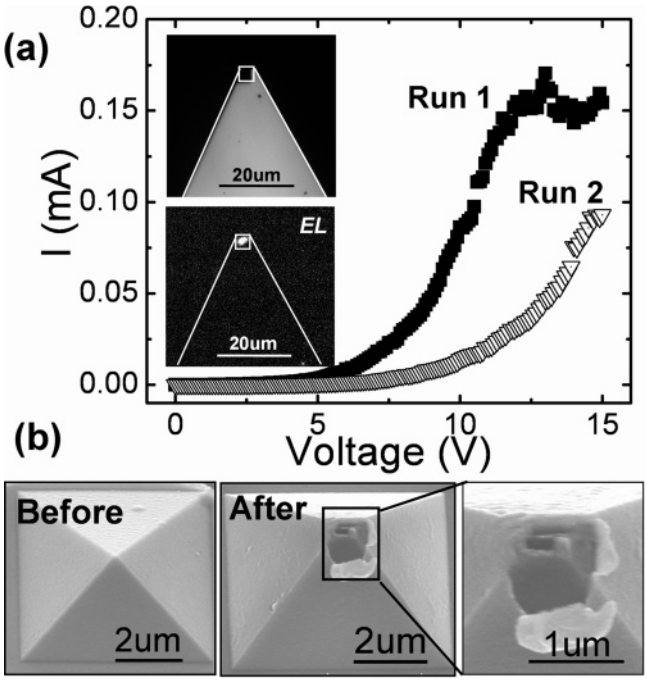

Figure 6. (a) (Upper inset) An optical micrograph of an organic light-emitting heterostructure device deposited on an AFM probe tip, shown under external illumination. (Lower inset) An optical micrograph of the same device under forward bias, shown with the external light source turned off. The EL signal was captured by a CCD camera through a 50× objective lens with an exposure time of 1 s. The emission area can be determined from the upper optical photograph by tracing the outline of the AFM cantilever. Main plot: the corresponding current−voltage ($I-V$) characteristic of the device obtained during the EL measurement. The current drop from the first scan to the second (labeled "Run 1" and "Run 2," respectively) is indicative of device degradation on some portions of the AFM probe. This degradation is revealed by electron microscopy to be most commonly at the vertex. (b) SEMs of the organic heterostructure device on the AFM probe tip, before and after test, as indicated. The melted area at the vertex is approximately 500 nm in diameter and is indicative of intense Joule heating caused by current funneling through the vertex. These images are representative of multiple experiments having similar outcomes.

nm), LiQ (2 nm), and Al top electrode (100 nm); actual layer thickness values are given, as calibrated. Electrons are injected from the top (bottom) electrode when a forward (reverse) bias is applied; holes are not injected to any appreciable extent. On the planar substrate, electron injection from the top-deposited electrode is favored ("forward bias" condition), most likely due to the injection sites created by the deposition of metal onto organic and which are absent at the bottom interface.[23] On the other hand, the $J-V$ curves under forward and reverse bias are nearly identical for the structure deposited on an AFM probe. This strongly suggests that the high electric field near the vertex assists electron injection from the bottom electrode. The fact that the current density through the layer structure on the probe is a factor of 10^3 higher than that on the planar substrate further indicates selective carrier injection on the nonplanar substrate. (This localization of injection can also be seen in Figure A in Supporting Information.) In other words, we conclude that this change in the current injection behavior of metal−

organic−metal multilayers is caused primarily by the nanoscale variation in substrate curvature and has important implications for the design of nanostructured organic devices. Here, it is utilized to achieve nanoscale localization of current injection and light emission.

Indeed, as shown in Figure 6, highly localized light emission is observed from this device in forward bias, as shown in the far-field optical images of the tip under external illumination (upper inset of Figure 6a) and in the dark (lower inset of Figure 6b), along with the corresponding current−voltage characteristics (Figure 6a). The location of the light emission area in lower inset of Figure 6b was determined by tracing the outline of the AFM cantilever and the shape of pyramid from the illuminated image (upper inset of Figure 6a). Note that the increased current density through the probe tip can also be visualized via the localized degradation of the OLED structure due to Joule heating, as seen in the scanning electron microscopy (SEM) images of Figure 6b. The melted region, that is, the darkened region on the vertex, measures less than 500 nm across, suggesting a comparably sized region of high-current injection and light emission. The size of the melted region is also consistent with the size of the charge recombination zone as would be predicted by the field distribution, roughly equal to the sum of the vertex diameter (100 nm) and the added thickness of the OLED device on either side of the vertex (2×175 nm). (Additional micrographs are available as Supporting Information.) In the far-field, however, the imaged size of the emissive region is diffraction limited. Further verification can be obtained via near-field optical techniques, which is the subject of our ongoing efforts.

In summary, in this article we describe a lithography-free process developed to fabricate an electrically pumped OLED on a pyramidal AFM tip, where the localization of charge injection, charge recombination, and light emission are achieved via the nonplanar substrate geometry. The current−voltage characteristics of tipless control devices and devices on tipped probes, along with the optical images of the probe tip emission, show that the device can be turned on just at the tip by selective current injection into the pyramid region. An inverted device structure was developed to further enhance the selective current injection, taking advantage of the highly concentrated electric field due to nanoscale curvature of the probe's vertex. Electron micrographs of the devices before and after electrical biasing show extensive Joule heating at the vertex of the tip, indicative of current funneling through a submicrometer-sized region. The ability to reliably fabricate nanoscale organic-based light sources on commercial AFM cantilever substrates without extensive postprocessing suggests applications in high-resolution scanning optical microscopy, as well as nanoscale optical and chemical sensing.

Acknowledgment. The authors acknowledge the Office of Naval Research (Contract N00014-05-1-0713) and the National Science Foundation (ECS-0523986) for their financial support of this work.

Supporting Information Available: Additional micrographs of similar devices. This material is available free of charge via the Internet at http://pubs.acs.org.

References

(1) Betzig, E.; Trautman, J. K. *Science* **1992**, *257* (5067), 189−195.
(2) Bachelot, R.; Lerondel, G.; Blaize, S.; Aubert, S.; Bruyant, A.; Royer, P. *Microsc. Res. Tech.* **2004**, *64* (5−6), 441−452.
(3) Dickson, W.; Stashkevitch, A.; Ben Youssef, J.; Takahashi, S.; Zayats, A. V. *Opt. Commun.* **2005**, *250* (1−3), 126−136.
(4) Mulin, D.; Girard, C.; Des Francs, G. C.; Spajer, M.; Courjon, D. *J. Microsc. Oxford* **2001**, *202* (1−3), 110−116.
(5) Bozhevolnyi, S. I.; Volkov, V. S.; Sondergaard, T.; Boltasseva, A.; Borel, P. I.; Kristensen, M. *Phys. Rev. B* **2002**, *66* (23), 235204.
(6) Zia, R.; Schuller, J. A.; Brongersma, M. L. *Phys. Rev. B* **2006**, *74*, 165415−1−12.
(7) Denyer, M.; Micheletto, R.; Nakajima, K.; Hara, M.; Okazaki, S. *J. Nanosci. Nanotechnol.* **2003**, *3* (6), 496−502.
(8) Betzig, E.; Chichester, R. J. *Science* **1993**, *262* (5138), 1422−1425.
(9) Hecht, B.; Sick, B.; Deckert, V.; Zenobi, R.; Martin, O.; Pohl, D. *J. Chem. Phys.* **2000**, *112* (18), 7761−774.
(10) Stahelin, M.; Bopp, M. A.; Tarrach, G. T.; Meixner, A. J.; Zschokke-Granacher, I. *Appl. Phys. Lett.* **1996**, *68* (19), 2603−2605.
(11) Dutoit, B.; Zeisel, D.; Deckert, V.; Zenobi, R. *J. Phys. Chem. B* **1997**, *101* (35), 6955−6959.
(12) Minh, P. N.; Ono, T.; Fsashi, M. *Fabrication of Silicon Microprobes for Optical Near Field Applications*; CRC Press: Boca Raton, FL, 2002.
(13) Sasaki, M.; Tanaka, K.; Hane, K. *Jpn. J. Appl. Phys., Part 1* **2000**, *39* (12B), 7150−7153.
(14) Heisig, S.; Rudow, O.; Oesterschulze, E. *Appl. Phys. Lett.* **2000**, *77* (8), 1071−1073.
(15) Iwata, N.; Wakayama, T.; Yamada, S. *Sens. Actuators., A* **2004**, *111* (1), 26−31.
(16) Kroemer, H. *J. Cryst. Growth* **1987**, *81* (1−4), 193−204.
(17) An, K. H.; Zhao, Y.; O'Connor, B.; Pipe, K. P.; Shtein, M. *Appl. Phys. Lett.* **2006**, *89* (11), 111117.
(18) Burrows, P. E.; Shen, Z.; Bulovic, V.; McCarty, D. M.; Forrest, S. R.; Cronin, J. A.; Thompson, M. E. *J. Appl. Phys.* **1996**, *79* (10), 7991−8006.
(19) Shtein, M.; Peumans, P.; Benziger, J. B.; Forrest, S. R. *J. Appl. Phys.* **2003**, *93* (7), 4004−4016.
(20) Kuttel, O. M.; Groening, O.; Emmenegger, C. E.; Schlapbach, L. *Appl. Phys. Lett.* **1998**, *73* (15), 2113−2115.
(21) Vaufrey, D.; Khalifa, M. B.; Tardy, J.; Ghica, C.; Blanchin, M. G.; Sandu, C.; Roger, J. A. *Semicond. Sci. Tech.* **2003**, *18* (4), 253−260.
(22) Parthasarathy, G.; Burrows, P. E.; Khalfin, V.; Kozlov, V. G.; Forrest, S. R. *Appl. Phys. Lett.* **1998**, *72* (17), 2138−2140.
(23) Ishii, H.; Sugiyama, K.; Ito, E.; Seki, K. *Adv. Mater.* **1999**, *11* (8), 605−625.

NL071883W